Journal of Hazardous Materials 180 (2010) 675–682

Contents lists available at ScienceDirect

Journal of Hazardous Materials

journal homepage: www.elsevier.com/locate/jhazmat

Photodegradation of acetone over V-Gd-O composite catalysts under visible light

Yiming He [a,*], Ying Wu [c], Tianlu Sheng [b], Xintao Wu [b,**]

[a] College of Mathematics, Physics and Information Engineering, Zhejiang Normal University, Jinhua, 321004, China
[b] State Key Laboratory of Structural Chemistry, Fujian Institute of Research on the Structure of Matter, Chinese Academy of Sciences, Fuzhou, 350002, China
[c] Institute of Physical Chemistry, Zhejiang Key Laboratory for Reactive Chemistry on Solid Surfaces, Zhejiang Normal University, Jinhua, 321004, China

ARTICLE INFO

Article history:
Received 31 January 2010
Received in revised form 22 March 2010
Accepted 22 April 2010
Available online 29 April 2010

Keywords:
Photodegradation
Photocatalyst
V_2O_5
$GdVO_4$
Acetone

ABSTRACT

A series of visible light active catalysts, V-Gd-O composites, were prepared by the impregnation method. In the photodegradation of acetone, the highest acetone conversion was obtained on $V_1Gd_1O_x$ catalyst under visible light. The physical and photophysical properties of the composite catalyst have been characterized by XRD, FT-IR, Raman, BET surface area, UV–vis diffuse reflectance spectra, and photoluminescence (PL) spectra. The characterization indicates the V-Gd-O photocatalyst exhibits three phases: Gd_2O_3, $GdVO_4$ and V_2O_5. On the basis of the calculated energy band positions and PL spectra, the high activity of the V-Gd-O catalysts could be attributed to the coupling effect between $GdVO_4$ and V_2O_5 in retarding the recombination of electron–hole pairs.

1. Introduction

The photocatalytic decomposition of pollutants in water and air has attracted much interest for several decades [1–2]. In terms of the high activity and chemical stability, TiO_2 is an excellent photocatalyst that can remove a large range of organic pollutants [3]. However, it is active only in ultraviolet (UV) region because its wide band gap (3.2 eV). Practically, this factor strongly limits the use of solar spectra as a source for the photoreaction. Hence, the visible light active photocatalyst is desired. Currently, there are two strategies to develop the visible light-driven photocatalysts: modification of TiO_2 [4–8] and exploitation of novel semiconductor materials [9,10]. The doping of transition metal (such as Fe^{3+}, Co^{3+}, Cr^{3+}, Ni^{3+}, Mo^{5+}, Re^{5+}, Ru^{3+}, W^{6+}) into TiO_2 could make TiO_2 show active under visible light. But they only make use of a limited visible light [4–6]. There are also reports on anion (such as N^{3-}, S^{2-}, C^{4-} and F^-) doped TiO_2 catalysts, which show activity under visible light. However, they are either unstable or only show low activity in the photodegradation of organic compounds [7,8]. The activities of modified TiO_2 catalysts in the visible light are limited. So, many investigations have been undertaken on the latter strategy. A great number of novel undoped single-phase mixed oxide semiconductor photocatalyts have been developed, such as $CaBi_2O_4$, $BiVO_4$, $BaBi_2Mo_4O_{16}$, Bi_2SbVO_7, and so on [10–14]. They all show a certain absorption in the visible light range. In general, these catalysts are synthesized by the conventional solid-state reactions between the corresponding oxides at high temperatures. So, they have some disadvantages such as small specific surface areas, long migration distances for excited electron–hole pairs, and increasing energy-wasteful recombination; all of these were expected to lower photocatalytic activities. It is reported that loading a small amount of noble metals (such as Pt, Ag, Pd) [15–17] and metal oxide (such as RuO_2, V_2O_5, Co_3O_4) [18–20] could improve the activity of these photocatalysts. The oxide doped catalysts named composite photocatalyst attract much attention because of its high-performance and low cost. However, some doping oxides can improve the photocatalytic performance, but others may debase it [16,19]. It is determined by the energy band structures, morphologies, and photoelectrochemical characteristics of the doping oxides and photocatalysts. So, designing more efficient visible light-driven composite photocatalytic materials is a challenging goal for the researchers and the extensive research work is needed.

Up to now, a large variety of composite semiconductors has been reported, such as $Co_3O_4/BiVO_4$, CdS/TiO_2, V_2O_5/MgF_2, and so on [20–24]. Almost all the metal or transition metal elements, which are usually in the forms of oxides, were included and studied. But the lanthanide is seldom used because the lanthanide-containing materials usually have the excellent luminescent properties and the photoexcited electron–hole pairs recombined fast in the materials [25–27]. In this paper, we present the explorative work about the photocatalytic performance of lanthanide-containing composite. A series of V-Ln-O (Ln = La, Nd, Sm, Eu, Gd, Dy, Ho, Yb)

* Corresponding author. Tel.: +86 0579 82283920; fax: +86 0579 82283920.
** Corresponding author. Tel.: +86 0591 83714946; fax: +86 0591 83714946.
E-mail addresses: hym@zjnu.cn (Y. He), wxt@fjirsm.ac.cn (X. Wu).

0304-3894/$ – see front matter © 2010 Elsevier B.V. All rights reserved.
doi:10.1016/j.jhazmat.2010.04.091

composite photocatalysts was synthesized by a simple method. The performance of these catalysts in acetone photodegradation was tested. The result shows V-Gd-O composite catalysts present high photocatalytic activity under visible light. In order to get an admissible explanation for the results, the specific areas, structures and photoadsorption ability of the V-Gd-O composite catalyst were characterized by BET, XRD, FT-IR and UV–vis technology.

2. Experimental

2.1. Catalyst preparation

NH_4VO_3 (>99%), Ln_2O_3 (>99.9%, Ln = La, Nd, Sm, Eu, Gd, Dy, Ho, Yb), and P25 (Degussa TiO_2) as reference, were purchased commercially and used without further purification. V_2O_5 was obtained by calcining ammonium metavanadate at 500 °C for 4 h. The $V_{0.2}Ln_1O_x$ (n_V/n_{Ln} = 0.2) catalysts were prepared by impregnation method. For the example of preparation of $V_{0.2}La_1O_x$ catalyst, 0.287 g of NH_4VO_3 was dissolved in 50 mL of H_2O to obtain a solution. Then 2.0 g of La_2O_3 was added under stirring. The water in the solution was evaporated slowly at 80 °C to obtain a solid mixture. After dried at 100 °C for 12 h, the mixture was calcined at 500 °C for 4 h and then cooled to room temperature to obtain the catalyst.

The V-Gd-O catalysts with different atomic ratio of vanadium and gadolinium (n_V/n_{Gd} = 0.2, 0.5, 0.8, 1.0, 1.5, 2.3, 3.0) were also prepared by the impregnation method listed above and calcined at 500 °C for 4 h.

$GdVO_4$ was prepared by the deposition method: Solution of NH_4VO_3 and solution of $Gd(NO)_3$ with a V to Gd mole ratio of 1.0 were mixed to obtain a deposit. The pH value of the solution was adjusted to 7–8 by a solution of NH_3H_2O. After aged at room temperature for 5 h, the deposit was filtrated, washed three times by water, dried at 100 °C for 12 h and calcined at 500 °C for 4 h.

V_2O_5/Gd_2O_3 (n_V/n_{Gd} = 0.8) catalyst was prepared by impregnation method and calcined at 300 °C for 4 h. $GdVO_4/Gd_2O_3$ (n_V/n_{Gd} = 0.8) was prepared by the following steps: 1.549 g of NH_4VO_3 was dissolved in 60 mL of H_2O to obtain solution A. 2.4 g of Gd_2O_3 was dissolved in 3.0 mL of concentrated nitric acid and 7.0 mL of H_2O to obtain solution B. Solution B was added into solution A under stirring. The PH of solution was adjusted to 7–8 by a solution of NH_3H_2O. Then 0.6 g of Gd_2O_3 was added. After aged at room temperature for 5 h, the deposit was filtrated, dried at 100 °C for 12 h and calcined at 500 °C for 4 h. $V_2O_5/GdVO_4$ (n_V/n_{Gd} = 1.5) was prepared by the similar steps: Solution of NH_4VO_3 and $Gd(NO_3)_3$ with a V to Gd mole ratio 1.5 were mixed and evaporated to give a solid precursor. After dried at 100 °C for 12 h, the solid precursor was calcined at 500 °C for 4 h and then cooled to room temperature to yield the catalyst.

2.2. Catalyst test

The catalytic reaction under UV light was carried out in a quartz tube (ID 5.0 mm) reactor and two 500 W high pressure mercury lamps were used as UV light sources. When it was carried out under visible light, the lamp and the reactor were changed. Two 400 W xenon lamps were used as visible light sources and a glass tube (ID 5.0 mm) reactor which could cut off most of the UV light was used. In each reaction, the bed length of catalyst was about 4.5 cm and the rest part of the reactors were wrapped by aluminum paper to exclude the contribution of the blank reaction (Fig. 1). A thermocouple which clung to the reactor closely was used to detect the reaction temperature. The reactor tube was cooled by a fan. Because of the heat from the lamps, even we tried to cool down the reactor by the fan, the temperature was still between

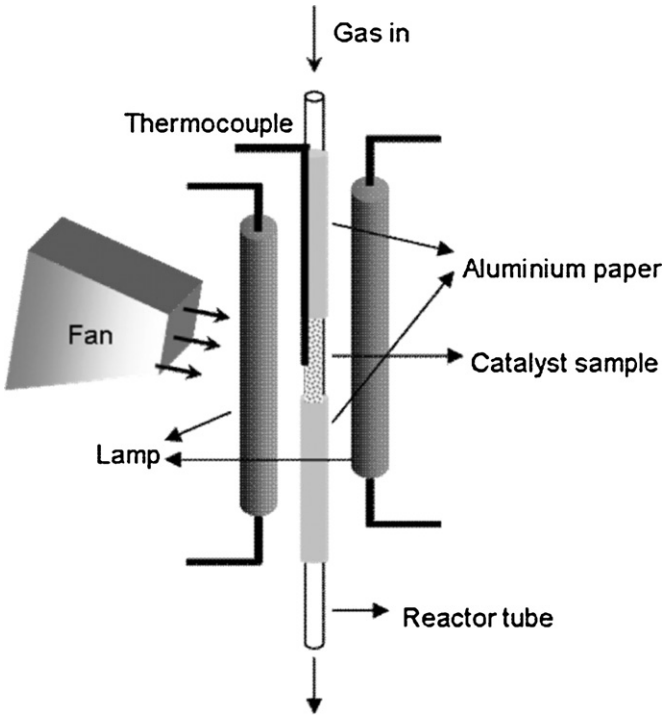

Fig. 1. The reactor system.

130 and 140 °C. Pure oxygen was used as the oxidants and the organic reactant is acetone. The organic substrate acetone was fed into the reactor by bubbling gas through liquid acetone at 0 °C (cooled in a water-ice bath) to obtain the reactant mixture. The flow of mixture was controlled at 8.0 mL/min. Before each catalytic testing, the photocatalyst was allowed to equilibrate in the reaction gas for at least 60 min. The reaction products were analyzed on a gas chromatograph (GC-950) with thermal conductor detectors and a gas chromatograph/mass spectrometer (Agilent 6890N/5973N). The catalyst activity and selectivity as well as the mol concentration of acetone (10%) were calculated by the area normalized method. All the data were collected after 3 h of online reaction.

In order to rule out the thermal reaction, the most activity catalyst $V_1Gd_1O_x$ was tested for acetone oxidation in dark at the same reaction temperature 140 °C. The dark reaction shows that acetone did not react with oxygen over $V_1Gd_1O_x$ catalysts at 140 °C. The blank reaction was also tested. The result shows that no acetone was photodegradated without photocatalyst under visible light.

2.3. Characterizations

The XRD characterization of catalysts was carried out on an X-ray diffraction spectroscopy meter (RIGAKU DMAX2500) using Cu Kα radiation (40 kV/40 mA). The specific surface areas (S_{BET}) of catalysts were measured by nitrogen adsorption on Autosorb-1 (Quantachrome Instruments). The Raman spectra of the catalysts were collected on RM1000 spectrometer (Renishaw) with an Ar ion laser (514.5 nm) as excitation source. The FT-IR spectra of catalysts were recorded on a FT-IR spectroscopy meter (Nicolet Magna 750) with a resolution of 4 cm^{-1}. The UV–vis spectra of catalysts were recorded on a UV–vis spectrometer (PerkinElmer Lambda900) equipped with an integrating sphere. The photoluminescence (PL) spectra of catalysts were collected on Horiba Jobin Yvon (FL3-P-TCSPC) instrument. The light source was a Xe lamp (excitation at 292 nm).

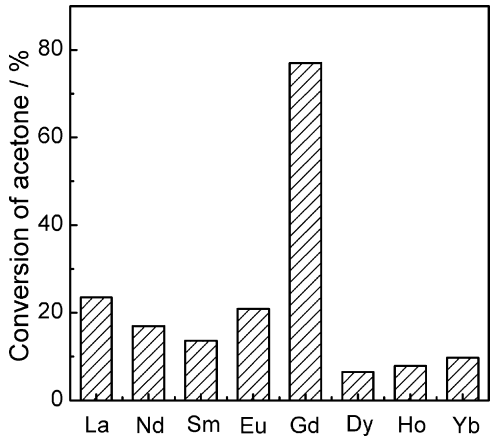

Fig. 2. Photoactivity of $V_{0.2}Ln_1O_x$ (Ln = La, Nd, Sm, Eu, Gd, Dy, Ho, Yb) catalysts on the degradation of acetone under UV light.

3. Results and discussion

3.1. Photocatalytic activity of the catalysts

The catalytic reactions were carried out in a reaction system as shown in Fig. 1. P25 (TiO_2 Degussa), V_2O_5, and Ln_2O_3 (Ln = La, Nd, Sm, Eu, Gd, Dy, Ho, Yb) were tested in the photodegradation reaction of acetone. Results are listed in Table 1. Under UV light, P25 had a high activity for acetone degradation. 99.1% of acetone conversion was obtained. But under visible light, P25 shows low activity like V_2O_5. Ln_2O_3 was inactive under visible light and only showed low acetone conversion under UV light.

Fig. 2 shows the photocatalytic activity of $V_{0.2}Ln_1O_x$ catalyst samples under UV light. As shown in Fig. 2, most of catalyst samples showed low acetone conversion except the $V_{0.2}Gd_1O_x$ catalyst. 77% acetone conversion was obtained over the $V_{0.2}Gd_1O_x$ catalyst under UV light. It means V-Gd-O catalyst might be a high-performance photocatalyst. With that in mind a series of V-Gd-O catalyst with different V/Gd atomic ratio were prepared and tested in the photodegradation reaction of acetone. The results are listed in Fig. 3a. Under UV light the acetone degradation conversion increased with an increase in V/Gd atomic ratio from 0 to 0.8 and decreased at even higher V/Gd ratio. The highest acetone conversion was obtained on catalyst $V_{0.8}Gd_1O_x$. The acetone conversion reached 98.7% under UV light. Under visible light the photoactivity of V-Gd-O catalysts showed the similar change trend. But the acetone conversion was lower than that under UV light. The highest acetone conversion (95.5%) was obtained on catalyst $V_1Gd_1O_x$ and it was stable within 24 h of online reaction (Fig. 3b). The results of Table 1 and Fig. 3 show that the V-Gd-O catalysts are more active than both Gd_2O_3 and V_2O_5. Obviously, doping of V_2O_5 to Gd_2O_3 formulated a series of active photodegradation catalysts.

In the photodegradation of acetone, the typical degradation products are CO_2, CO, acetol, and H_2O. As an example, for the photodegradation of acetone over $V_1Gd_1O_x$ catalyst sample, the selectivities to CO_2, CO, and acetol are 40.2%, 52.9%, and 6.9%, respectively. There is a significant amount of CO and acetol left as partial oxidation products which are still viewed as a pollutant. This disadvantage could be made up by doping a little amount of Pt. Higher photocatalytic activity (99.4% conversion of acetone) was obtained over 0.1 wt% $Pt/V_1Gd_1O_x$ catalyst and only CO_2 and H_2O were detected in the products. The above results indicate the V-Gd-O composite photocatalyst is promising for practical application in air purification.

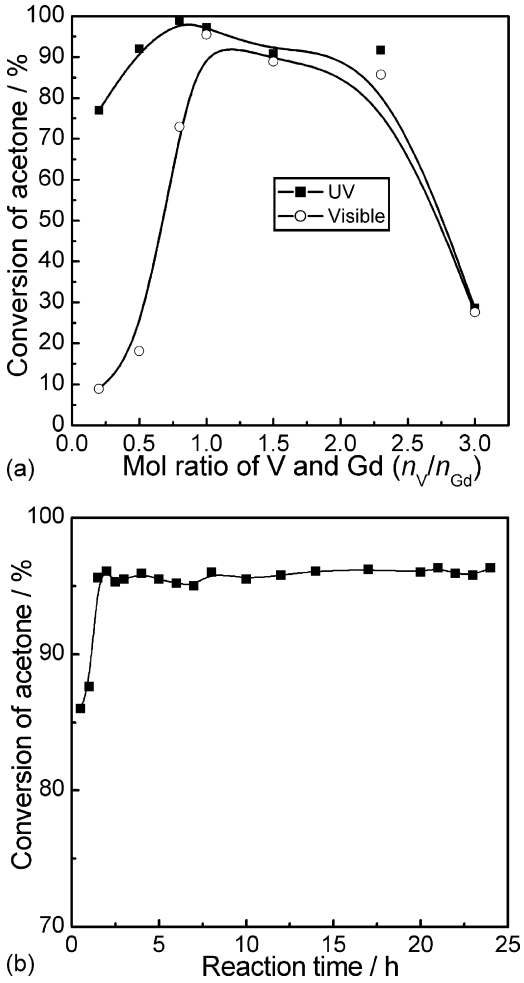

Fig. 3. Activities of catalysts on photodegradation of acetone. (a) V-Gd-O catalysts with different V/Gd ratio, (b) life-testing of $V_1Gd_1O_x$ catalyst under visible light irradiation.

3.2. Characterization of the catalysts

The specific surface area of catalyst might be a factor to influence activity of the catalysts. Table 2 shows the specific surface areas of P25, V_2O_5, Gd_2O_3, and V-Gd-O catalysts. P25 has a large surface area of 52 m^2/g, which might be one of the reasons for its high activity. Unlike P25, V_2O_5 and Gd_2O_3 show low surface areas. V-Gd-O catalysts also have low specific surface areas and no obvious regulation was observed with the change of V/Gd atomic ratio.

Fig. 4 presents the XRD patterns of V-Gd-O catalysts with different V/Gd atomic ratio. Pure Gd_2O_3 shows several strong diffraction peaks at $2\theta = 20.0^\circ, 28.5^\circ, 33.0^\circ, 47.4^\circ$ (JCPDS 12-0797). When vanadium was doped into Gd_2O_3 several new peaks at $2\theta = 18.5^\circ, 24.7^\circ, 49.0^\circ$ appeared, which could be assigned to tetragonal phased $GdVO_4$ (JCPDS 17-0260). With the increase in vanadium concentration, the peak intensity of $GdVO_4$ increased. But when the V/Gd atomic ratio was higher than 1.0, little changes were observed. Besides $GdVO_4$ phase, V_2O_5 was also observed in the V-Gd-O catalysts. As shown in Fig. 4, when the V/Gd molar ratio is increased to 0.5, the peak of V_2O_5 appeared. With the further increase of vanadium concentration, the peak of V_2O_5 became sharper and stronger.

The results of XRD experiment indicate that V-Gd-O catalyst was composed by Gd_2O_3, $GdVO_4$ and V_2O_5 phase. It was also proved by FT-IR experiment. Fig. 5 shows the FT-IR spectra of V-Gd-O catalysts with different V/Gd atomic ratio. As shown in Fig. 5, Gd_2O_3 has

Table 1
Photodegradation of acetone over different catalysts.

Catalyst	P25	V_2O_5	La_2O_3	Nd_2O_3	Sm_2O_3	Eu_2O_3	Gd_2O_3	Dy_2O_3	Ho_2O_3	Yb_2O_3
X_{UV} (%)	99.1	12.2	6.1	3.6	4.5	4.5	8.9	5.1	3.0	2.4
X_{Vis} (%)	14.5	10.2	–	–	–	–	–	–	–	–

Note: X_{UV} represents the conversion of acetone under UV light, X_{Vis} represents the conversion of acetone under visible light.

a broad peak at 541 cm^{-1}. Over V-Gd-O catalyst two other peaks were observed besides the peak of Gd_2O_3. One peak was located at 785 cm^{-1}, which could be assigned to $GdVO_4$ phase [28]. Another peak was located at 1021 cm^{-1}, which could be assigned to the V=O stretching vibration in V_2O_5 phase [29]. With the increase of V/Gd atomic ratio, the peak of V_2O_5 became stronger at the expense of the peak of Gd_2O_3. The FT-IR characterizations are consistent to those of XRD shown in Fig. 4.

Table 2
Specific surface areas of P25 and V-Gd-O catalysts.

Catalysts	S ($m^2\ g^{-1}$)	Catalysts	S ($m^2\ g^{-1}$)
P25	52	$V_{0.8}Gd_1O_x$	7
V_2O_5	6	$V_1Gd_1O_x$	6
Gd_2O_3	3	$V_{1.5}Gd_1O_x$	7
$V_{0.2}Gd_1O_x$	5	$V_{2.3}Gd_1O_x$	7
$V_{0.5}Gd_1O_x$	6	$V_{3.0}Gd_1O_x$	6

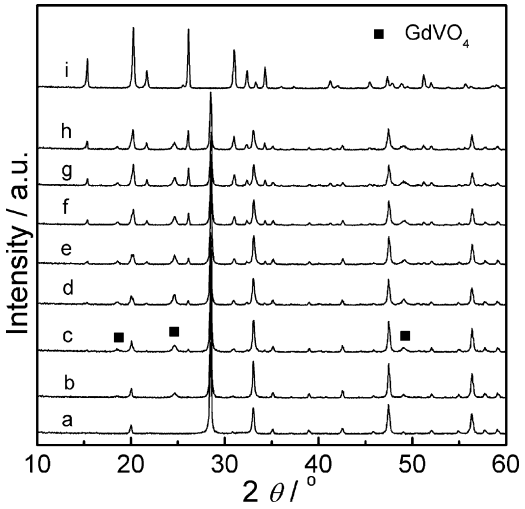

Fig. 4. XRD patterns of Gd_2O_3 (a), V_2O_5 (i) and V-Gd-O catalysts, (b) $V_{0.2}Gd_1O_x$; (c) $V_{0.5}Gd_1O_x$; (d) $V_{0.8}Gd_1O_x$; (e) $V_1Gd_1O_x$; (f) $V_{1.5}Gd_1O_x$; (g) $V_{2.3}Gd_1O_x$; (h) $V_{3.0}Gd_1O_x$.

Fig. 6 shows the Raman spectra of Gd_2O_3, V_2O_5, and catalysts with different vanadium concentrations. Gd_2O_3 (Fig. 6, curve a) has several strong peaks at 218, 359, 552, 728, 940, and 1021 cm^{-1}, while V_2O_5 (Fig. 6, curve i) shows several strong peaks at 142, 282, 403, 526, 699, 992 cm^{-1}. When V_2O_5 was doped to Gd_2O_3, two new peaks at 821 and 882 cm^{-1} which could be assigned to $GdVO_4$ appeared. Besides, the peak corresponding to V_2O_5 phase was also observed. At relatively lower vanadium concentrations (V/Gd molar ratio was lower than 0.8:1), the Raman bands of $GdVO_4$ are stronger than those of V_2O_5. With the increase of vanadium concentration, the peak intensity of V_2O_5 increased. The results in Fig. 6 indicate that all of the V-Gd-O catalysts have peaks that could be assigned to Gd_2O_3, $GdVO_4$, and V_2O_5. It is consistent with the results of XRD and FT-IR experiments.

Fig. 7 presents the UV–vis spectra of Gd_2O_3, P25, V_2O_5, and V-Gd-O catalysts. As shown in Fig. 7, both Gd_2O_3 and P25 could only absorb the UV light, while V_2O_5 could absorb most of the visible light. The V-Gd-O catalysts show stronger photoabosorption performance than Gd_2O_3 or P25 in the visible region. With the increase of V/Gd atomic ratio, the photoabsorption performance of V-G-O catalysts increased. Based on the results of XRD, Raman, and FT-IR experiment, it is obvious that the increased photoabsorption performance in the visible region is due to the increased V_2O_5 phases in the V-Gd-O composite catalysts.

3.3. Discussion

The composite photocatalysts have attracted increasing attention for their enhanced performance. Yet present explanations are still far from clarifying it. Some researchers attribute the increased activity to the adsorption ability for the organic compounds, which are often related to the specific surface area [30,31]. In the present paper, all the V-Gd-O catalysts show low specific surface areas and little difference was observed. Considering that these samples have the similar phase composition, we think the change in adsorption

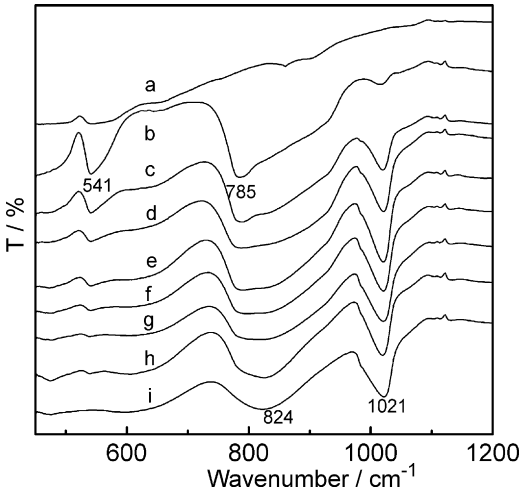

Fig. 5. FT-IR spectra of Gd_2O_3 (a), V_2O_5 (i) and V-Gd-O catalysts, (b) $V_{0.2}Gd_1O_x$; (c) $V_{0.5}Gd_1O_x$; (d) $V_{0.8}Gd_1O_x$; (e) $V_1Gd_1O_x$; (f) $V_{1.5}Gd_1O_x$; (g) $V_{2.3}Gd_1O_x$; (h) $V_{3.0}Gd_1O_x$.

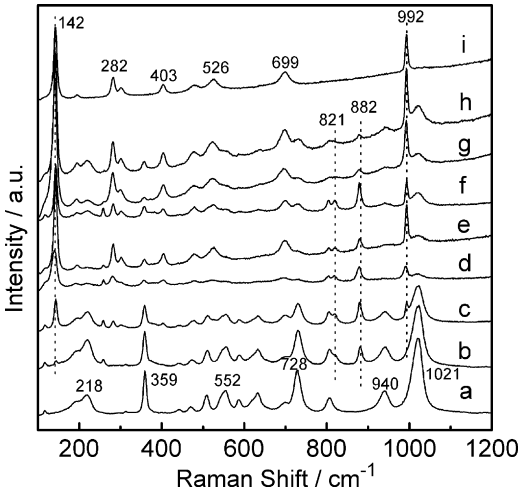

Fig. 6. Raman spectra of Gd_2O_3 (a), V_2O_5 (i) and V-Gd-O catalysts, (b) $V_{0.2}Gd_1O_x$; (c) $V_{0.5}Gd_1O_x$; (d) $V_{0.8}Gd_1O_x$; (e) $V_1Gd_1O_x$; (f) $V_{1.5}Gd_1O_x$; (g) $V_{2.3}Gd_1O_x$; (h) $V_{3.0}Gd_1O_x$.

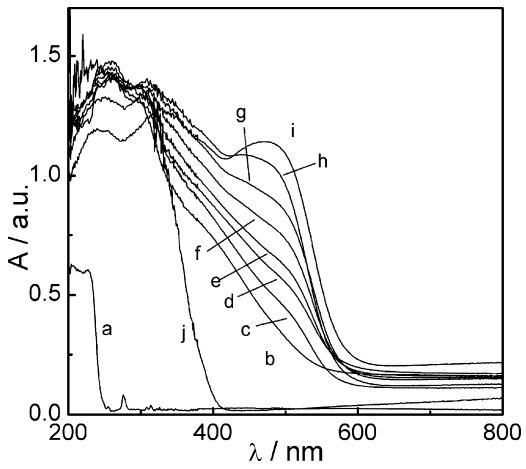

Fig. 7. UV–vis spectra of Gd_2O_3 (a), V_2O_5 (i), P25 (j) and V/Gd_2O_3 catalysts: (b) $V_{0.2}Gd_1O_x$; (c) $V_{0.5}Gd_1O_x$; (d) $V_{0.8}Gd_1O_x$; (e) $V_1Gd_1O_x$; (f) $V_{1.5}Gd_1O_x$; (g) $V_{2.3}Gd_1O_x$; (h) $V_{3.0}Gd_1O_x$.

ability is not a major factor to influence the photoactivity of V-Gd-O catalysts. The most important factor might be the composition of the catalysts.

Different measures of characterizations have indicated that V-Gd-O catalysts are composed by V_2O_5, Gd_2O_3, and $GdVO_4$. Gd_2O_3 was inactive in the visible region, and V_2O_5 shows low activity. $GdVO_4$ was a new phase formed during the calcination process. To the best of our knowledge, previously there have been no literatures focused on the photocatalytic performance of $GdVO_4$. In order to elucidate the mechanism in the V-Gd-O catalysts, pure $GdVO_4$ (tetragonal phase, consistent with JCPDS 17-0260) was prepared by deposition method and calcined at 500 °C for 4 h. Fig. 8a shows the UV–vis spectra of $GdVO_4$. The band gap absorption edge of pure $GdVO_4$ is determined to be 516 nm, corresponding to the band gap (E_g) energy 2.40 eV (estimated by Kubelka Munk formula, Fig. 8b). By the same way, the E_g of Gd_2O_3 and V_2O_5 can be estimated to be 5.09 and 2.06 eV, respectively (Fig. 8b). $GdVO_4$ has a much smaller band gap than Gd_2O_3 and could absorb the visible light like V_2O_5. Actually, many vanadate salts have a large band gap and show white color. But when the introduced cation has a $d^{10}s^0$ electron configuration or has the partially filled 4f orbitals, the electronic structure of the vanadate is usually changed and a decrease in the band gap would be realized (such as $BiVO_4$ (E_g = 2.8 eV) [20], $EuVO_4$ (E_g = 1.9 eV) [32] and $CeVO_4$ (E_g = 1.8 eV) [33]). Due to the same reason, $GdVO_4$ could absorb the visible light like $CeVO_4$. The photocatalytic performance of pure $GdVO_4$ was also investigated. 60.6% acetone conversion was obtained under visible light. This result shows that the photoactivity of $GdVO_4$ is stronger than that of V_2O_5 and Gd_2O_3, but lower than that of V-Gd-O catalysts.

So, all the single-phase samples did not show high activity, but when they were combined together, the enhanced photocatalytic activity was obtained. Many researchers have noted the particularity of the photoactivity of composite systems consisting of two or three semiconductors in contact [19–24]. They attributed the improvement of activity to the enhanced charge separation, which is due to the electron or hole transfer between the coupled semiconductors. For example, in CdS/TiO_2 catalyst the photogenerated electrons on the conduction band of the CdS transfer to that of the TiO_2, and simultaneous holes on the valence band of TiO_2 can be transferred to that of CdS under the potential of band energy difference. Therefore, the recombination of electron–hole pairs can be reduced, and the photocatalytic reaction can be enhanced greatly [21].

In the current case, we think this mechanism also works. Because all of V_2O_5, Gd_2O_3, and $GdVO_4$ were observed in the V-Gd-O catalysts, there might exist three possible combinations (V_2O_5 and Gd_2O_3, Gd_2O_3 and $GdVO_4$, or V_2O_5 and $GdVO_4$). However, the charge migration would not occur between every two semiconductors. They should have the suitable potential of the band energy. That means the migration direction of the photogenerated charge carrier depends on the band edge positions of the two semiconductors. Base on the literatures reported [34,35], we know that the band edge positions could be predicted theoretically from the absolute (or Mulliken) electronegativity. The conduction band edge of a semiconductor at the point of zero charge (pH_{zpc}) can be predicted by Eq. (1):

$$E^0_{CB} = X - E_c - 1/2\,E_g \quad (1)$$

where X is the absolute electronegativity of the semiconductor, expressed as the geometric mean of the absolute electronegativity of the constituent atoms, which is defined as the arithmetic mean of the atomic electron affinity and the first ionization energy; E_c is the energy of free electrons on the hydrogen scale (~4.5 eV); and E_g is the band gap of the semiconductor. The predicted band edge positions of Gd_2O_3, V_2O_5 and $GdVO_4$ by the above equation are shown in Table 3. In fact, these values are slightly more anodic than the measured value but this does not affect the comparison of their relative positions. As shown in Table 3, the conduction band position of

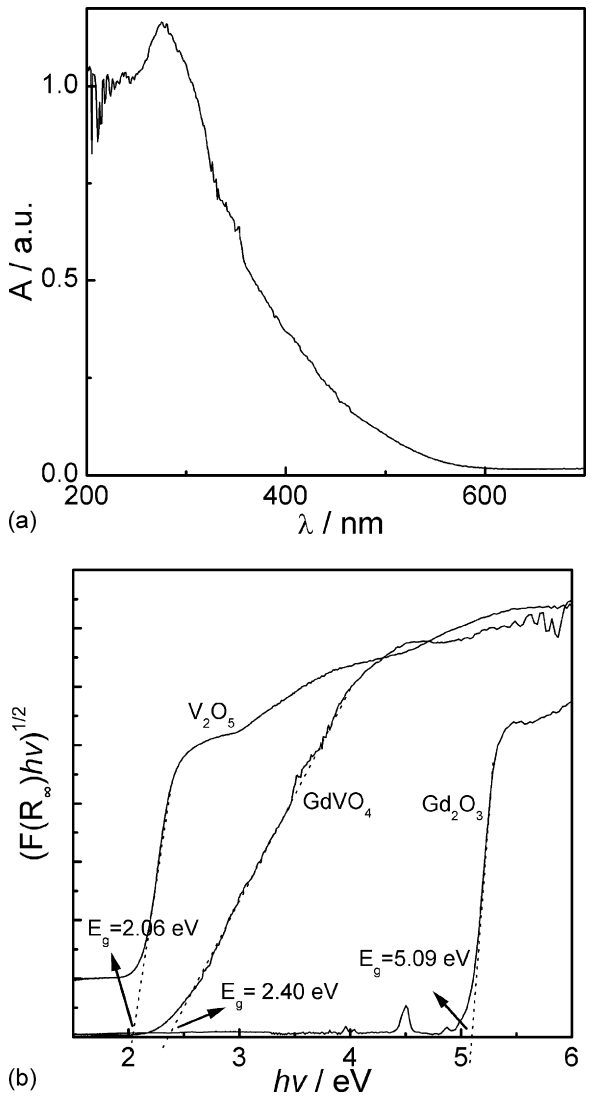

Fig. 8. UV–vis spectra of (a) $GdVO_4$ and (b) estimated band gap of photocatalysts by Kubelka Munk function.

Table 3
Absolute electronegativity, estimated band gap, energy levels of calculated conduction band edge, and valence band at the point of zero charge for Gd_2O_3, V_2O_5, $GdVO_4$.

Semiconductor oxides	Absolute electronegativity (X)	Estimated energy band gap E_g (eV)	Calculated conduction band edge (eV)	Calculated valence band edge (eV)
Gd_2O_3	4.7625	5.09	−2.28	2.80
V_2O_5	6.4817	2.06	0.95	3.01
$GdVO_4$	5.7006	2.40	0.00	2.40

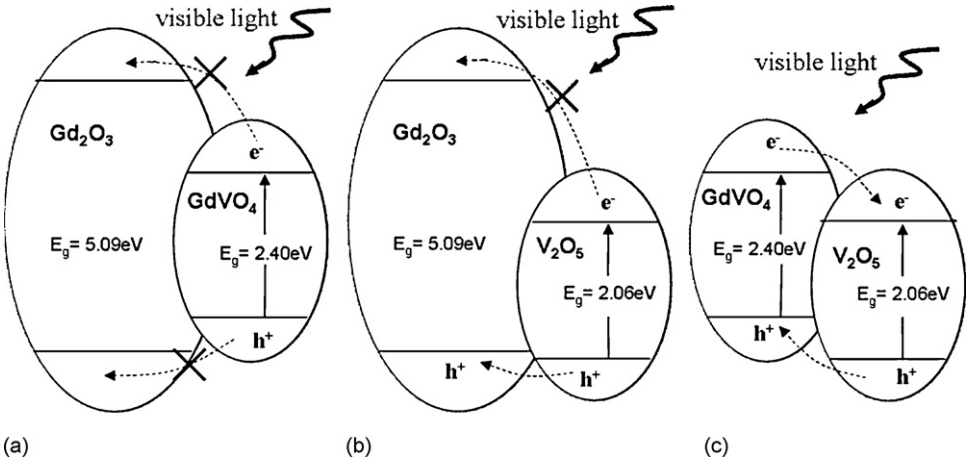

Fig. 9. Proposed principle of charge separation for V-Gd-O composite photocatalysts under visible light irradiation.

Gd_2O_3 is more cathodal than $GdVO_4$ and the valence band position of Gd_2O_3 is more anodic than $GdVO_4$. It means both the electron or hole transfer from the $GdVO_4$ to Gd_2O_3 is forbidden (Fig. 9a). There has not the coupling effect between $GdVO_4$ and Gd_2O_3. For the V_2O_5/Gd_2O_3 system (Fig. 9b), the valence band of V_2O_5 is more anodic than Gd_2O_3 and the hole transfer from the V_2O_5 to Gd_2O_3 is permitted. It could prolong the life of charges in some degree. However, the separation efficiency might be low because of the small difference in potential. The $V_2O_5/GdVO_4$ system (Fig. 9c) shows the highest separation efficiency. Their valence and conduction bands are suitably disposed and the difference in potential is large. The excited electron could transfer from the $GdVO_4$ to V_2O_5 easily, while the holes could transfer from the V_2O_5 to $GdVO_4$. The simultaneously charge transfer retards the recombination of electron–hole pairs and promoted photocatalytic activity greatly.

The above analysis shows that Gd_2O_3 phase has little promotion effect for the high activity and could be considered as an 'observer' in the V-Gd-O catalysts. The $GdVO_4$ and V_2O_5 are the active phases. The high activity of V-Gd-O catalysts could be attributed to the coupling effect between $GdVO_4$ and V_2O_5. In order to prove the above suggestion, we prepared three new catalysts with different phase compositions and tested their photocatalytic activity for acetone degradation under visible light. Fig. 10 shows the XRD patterns of the three catalysts. As shown in Fig. 10, the three catalysts could be denoted as V_2O_5/Gd_2O_3 ($x = 0.8$), $GdVO_4/Gd_2O_3$ ($x = 0.8$), and $V_2O_5/GdVO_4$ ($x = 1.5$) based on their phase composition (x represents the molar ratio of vanadium to gadolinium). Table 4 shows the photocatalytic activities of catalysts samples. Both V_2O_5/Gd_2O_3 ($x = 0.8$) and $GdVO_4/Gd_2O_3$ ($x = 0.8$) catalysts show low activity under visible light, although they have the same V/Gd atomic ratio with $V_{0.8}Gd_1O_x$ catalyst. On the other hand, $V_2O_5/GdVO_4$ ($x = 1.5$) catalyst shows higher acetone conversion than $V_{1.5}Gd_1O_x$ catalyst. Obviously, in the $V_2O_5/GdVO_4$ composite the recombination of excited electron–hole pairs is retarded effectively.

The PL spectra of $GdVO_4$, $Gd_2O_3/GdVO_4$ ($x = 0.8$), and $V_2O_5/GdVO_4$ ($x = 1.5$) catalysts support another proof (Fig. 11). The photoluminescence spectra of the photocatalysts are useful to disclose the migration, transfer, and recombination processes of the photogenerated electron–hole pairs in the semiconductor [36]. At room temperature the PL peaks of Gd_2O_3 and V_2O_5 between 430 and 650 nm are very weak and can be ignored. Tetraganol phased $GdVO_4$ has an obvious peak at around 500 nm in the PL spectrum, indicating that the electrons and holes recombine rapidly [37,38]. For $Gd_2O_3/GdVO_4$ ($x = 0.8$) catalyst, the PL peak is still strong. The slight decrease in intensity might be due to the decreased con-

Table 4
The photocatalytic activities of catalysts samples ($x = n_V/n_{Gd}$) under visible light.

Catalyst	Conv. (%)
V-Gd-O ($x = 0.8$)	72.9
Gd_2O_3/V_2O_5 ($x = 0.8$)	28.4
$Gd_2O_3/GdVO_4$ ($x = 0.8$)	5.9
V-Gd-O ($x = 1.5$)	88.9
$GdVO_4/V_2O_5$ ($x = 1.5$)	99.2

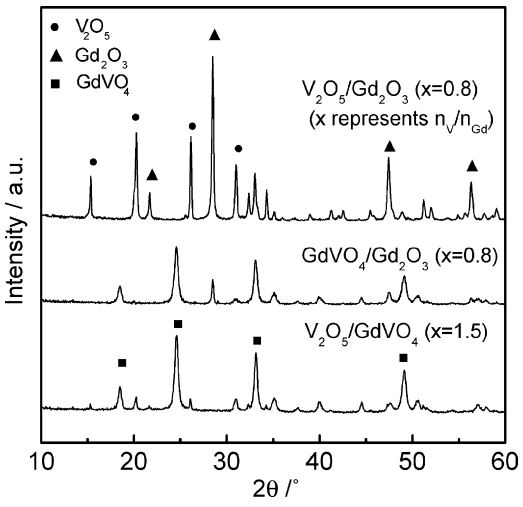

Fig. 10. XRD patterns of catalyst samples ($x = n_V/n_{Gd}$).

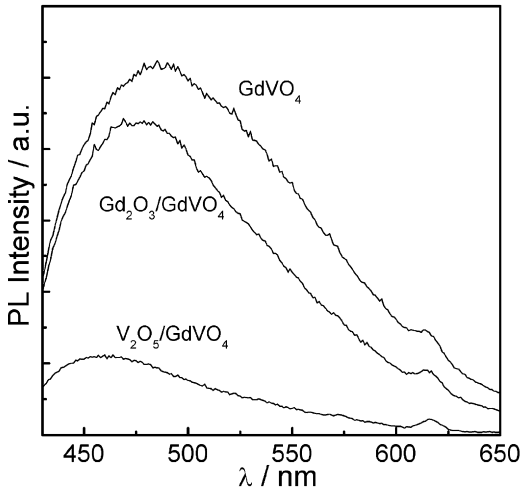

Fig. 11. PL spectra of photocatalysts.

centration of $GdVO_4$. However, over $V_2O_5/GdVO_4$ ($x = 1.5$) catalyst, the peak is weakened greatly, which could not be explained by the decrease of $GdVO_4$ concentration. It suggested that the doped V_2O_5 retarded the electron–hole pair recombination.

4. Conclusions

In conclusion, the visible light active V-Gd-O composite catalyst was prepared by impregnation method. Among them the $V_1Gd_1O_x$ catalyst shows the highest photocatalytic activity and 95.5% acetone conversion was obtained under visible light. The structure characterizations indicated that the V-Gd-O catalyst was composed by Gd_2O_3, V_2O_5 and $GdVO_4$ phases. By calculated energy band positions and PL spectra, it could be concluded that Gd_2O_3 is an observer, while the V_2O_5 and $GdVO_4$ are the active phase. The high activity of V-Gd-O catalyst could be attributed to the coupling effect between V_2O_5 and $GdVO_4$ and the decreasing recombination of photogenerated electron–hole pairs. So, the $V_2O_5/GdVO_4$ composite might show higher photocatalytic activity and this idea could be used to design new photocatalyst such as $V_2O_5/SmVO_4$ and $V_2O_5/EuVO_4$.

Acknowledgements

This work was supported by grants from the 973 Program (2007CB815301 and 2006CB932904), the National Science Foundation of China (20333070, 20673118, and 20871114), the Science Foundation of CAS (KJCX2-YW-M05) and of Zhejiang Education Department (Y200909374), the Research Initiation Funds for the Doctor of Zhejiang Normal University (ZC304008169) and the Technology Funds of Jinhua (2009-1-169).

References

[1] A. Fujishima, K. Honda, Electrochemical photolysis of water at a semiconductor electrode, Nature 238 (1972) 37–38.
[2] J.H. Carey, J. Lawrence, H.M. Tosine, Photodechlorination of PCB's in the presence of titanium dioxide in aqueous suspensions, Bull. Environ. Contam. Toxicol. 16 (1976) 697–701.
[3] A. Fujishima, T.N. Rao, D.A. Tryk, Titanium dioxide photocatalysis, J. Photochem. Photobiol. C: Photochem. Rev. 1 (2000) 1–21.
[4] W. Choi, A. Termin, M.R. Hoffmann, The role of metal ion dopants in quantum-sized TiO_2: correlation between photoreactivity and charge carrier recombination dynamics, J. Phys. Chem. 98 (1994) 13669–13679.
[5] D. Chatterjee, S. Dasgupta, Visible light induced photocatalytic degradation of organic pollutants, J. Photochem. Photobiol. C: Photochem. Rev. 6 (2005) 186–205.
[6] B.S. Liu, X.L. Wang, G.F. Cai, L.P. Wang, Y.B. Song, X.J. Zhao, Low temperature fabrication of V-doped TiO_2 nanoparticles, structure and photocatalytic studies, J. Hazard. Mater. 169 (2009) 1112–1118.
[7] R. Ashi, T. Morikawa, T. Ohwaki, K. Aoki, Y. Taga, Visible-light photocatalysis in nitrogen-doped titanium oxides, Science 293 (2001) 269–271.
[8] S. Sakthivel, H. Kisch, Daylight photocatalysis by carbon-modified titanium dioxide, Angew. Chem., Int. Ed. 42 (2003) 4908–4911.
[9] A. Kudo, H. Kato, I. Tsuji, Strategies for the development of visible-light-driven photocatalysts for water splitting, Chem. Lett. 33 (2004) 1534–1539.
[10] J.W. Tang, Z.G. Zou, J.H. Ye, Efficient photocatalytic decomposition of organic contaminants over $CaBi_2O_4$ under visible-light irradiation, Angew. Chem., Int. Ed. 43 (2004) 4463–4466.
[11] A. Kudo, K. Ueda, H. Kato, I. Mikami, Photocatalytic O_2 evolution under visible light irradiation on $BiVO_4$ in aqueous $AgNO_3$ solution, Catal. Lett. 53 (1998) 229–230.
[12] S. Tokunaga, H. Kato, A. Kudo, Selective preparation of monoclinic and tetragonal $BiVO_4$ with Scheelite structure and their photocatalytic properties, Chem. Mater. 13 (2001) 4624–4628.
[13] B. Muktha, G. Madras, T.N. Guru Row, A novel scheelite-like structure of $BaBi_2Mo_4O_{16}$: Photocatalysis and investigation of the solid solution, $BaBi_2Mo_{4-x}W_xO_{16}$ ($0.25 \le x \le 1$), J. Photochem. Photobiol. A: Chem. 187 (2007) 177–185.
[14] J.F. Luan, B.C. Pan, Y. Paz, Y.M. Li, X.S. Wu, Z.G. Zou, Structural, photophysical and photocatalytic properties of new Bi_2SbVO_7 under visible light irradiation, Phys. Chem. Chem. Phys. 11 (2009) 6289–6298.
[15] T. Ishihara, N.S. Baik, N. Ono, H. Nishiguchi, Y. Takita, Effects of crystal structure on photolysis of H_2O on K–Ta mixed oxide, J. Photochem. Photobiol. A: Chem. 167 (2004) 149–157.
[16] T. Ohno, S. Izumi, K. Fujihara, M. Matsumura, Electron–hole recombination via reactive intermediates formed on PdO-doped $SrTiO_3$ electrodes. Estimation from comparison of photoluminescence and photocurrent, J. Photochem. Photobiol. A: Chem. 129 (1999) 143–146.
[17] F. Han, V.S.R. Kambala, M. Srinivasanc, D. Rajarathnamc, R. Naidu, Tailored titanium dioxide photocatalysts for the degradation of organic dyes in wastewater treatment: a review, Appl. Catal. A: Gen. 359 (2009) 25–40.
[18] Y.M. He, Y. Wu, H. Guo, L.S. Tian, X.T. Wu, Visible light photodegradation of organics over VYO composite catalyst, J. Hazard. Mater. 169 (2009) 855–860.
[19] K. Teramura, K. Maeda, T. Saito, T. Takata, N. Saito, Y. Inoue, K. Domen, Characterization of ruthenium oxide nanocluster as a cocatalyst with $(Ga_{1-x}Zn_x)(N_{1-x}O_x)$ for photocatalytic overall water splitting, J. Phys. Chem. B 109 (2005) 21915–21921.
[20] M.C. Long, W.M. Cai, J. Cai, B.X. Zhou, X.Y. Chai, Y.H. Wu, Efficient photocatalytic degradation of phenol over $Co_3O_4/BiVO_4$ composite under visible light irradiation, J. Phys. Chem. B 110 (2006) 20211–20216.
[21] N. Serpone, P. Maruthamuthu, P. Pichat, E. Pelizzetti, H. Hidaka, Exploiting the interparticle electron transfer process in the photocatalysed oxidation of phenol, 2-chlorophenol and pentachlorophenol: chemical evidence for electron and hole transfer between coupled semiconductors, J. Photochem. Photobiol. A: Chem. 85 (1995) 247–255.
[22] Y.M. He, L.S. Tian, Y. Wu, J.S. Chen, R.B. Fu, S.M. Hu, X.T. Wu, Visible light-induced degradation of acetone over $SO_4^{2-}/MoO_x/MgF_2$ catalysts, J. Hazard. Mater. 168 (2009) 551–554.
[23] F. Chen, T.H. Wu, X.P. Zhou, The photodegradation of acetone over VO_x/MgF_2 catalysts, Catal. Commun. 9 (2008) 1698–1703.
[24] F. Chen, J. Wang, J.Q. Xu, X.P. Zhou, Visible light photodegradation of organic compounds over V_2O_5/MgF_2 catalyst, Appl. Catal. A: Gen. 348 (2008) 54–59.
[25] C.C. Yu, M. Yu, C.X. Li, X.M. Liu, J. Yang, P.P. Yang, J. Lin, Facile sonochemical synthesis and photoluminescent properties of lanthanide orthophosphate nanoparticles, J. Solid State Chem. 182 (2009) 339–347.
[26] L. Tsonev, Luminescent activation of planar optical waveguides in $LiNbO_3$ with rare earth ions Ln^{3+} – a review, Opt. Mater. 30 (2008) 892–899.
[27] J.G. Bünzli, S. Comby, A. Chauvin, C.D.B. Vandevyver, New opportunities for lanthanide luminescence, J. Rare Earths 25 (2007) 257–274.
[28] G.Z. Li, Z.L. Wang, M. Yu, Z.W. Quan, J. Lin, Fabrication and optical properties of core-shell structured spherical $SiO_2@GdVO_4:Eu^{3+}$ phosphors via sol–gel process, J. Solid State Chem. 179 (2006) 2698–2706.
[29] T. Ono, Y. Tanaka, T. Takeuchi, K. Yamamoto, Characterization of K-mixed V_2O_5 catalyst and oxidative dehydrogenation of propane on it, J. Mol. Catal. A: Chem. 159 (2000) 293–300.
[30] M.E. Simonsen, H. Jensen, Z.S. Li, E.G. Søgaard, Surface properties and photocatalytic activity of nanocrystalline titania films, J. Photochem. Photobio. A: Chem. 200 (2008) 192–200.
[31] Y. Chena, D.D. Dionysiou, A comparative study on physicochemical properties and photocatalytic behavior of macroporous TiO_2-P25 composite films and macroporous TiO_2 films coated on stainless steel substrate, Appl. Catal. A: Gen. 317 (2007) 129–137.
[32] M. Prasad, A.K. Pandit, T.H. Ansaril, R.A. Singh, B.M. Wanklyn, Electrical transport properties of $EuVO_4$ single crystal, Phys. Lett. A 138 (1989) 61–64.
[33] M.R. Dolgos, A.M. Paraskos, M.W. Stoltzfus, S.C. Yarnell, P.M. Woodward, The electronic structures of vanadate salts: cation substitution as a tool for band gap manipulation, J. Solid State Chem. 182 (2009) 1964–1971.
[34] M.A. Butler, D.S. Ginley, Prediction of flatband potentials at semiconductor-electrolyte interfaces from atomic electronegativities, J. Electrochem. Soc. 125 (1978) 228–232.

[35] Y. Xu, M.A.A. Schoonen, The absolute energy positions of conduction and valence bands of selected semiconducting minerals, Am. Mineral. 85 (2000) 543–556.
[36] J.W. Tang, Z.G. Zou, J.H. Ye, Photophysical and photocatalytic properties of $AgInW_2O_8$, J. Phys. Chem. B 107 (2003) 14265–14269.
[37] X.Z. Li, F.B. Li, C.L. Yang, W.K. Ge, Photocatalytic activity of WO_x–TiO_2 under visible light irradiation, J. Photochem. Photobiol. A: Chem. 141 (2001) 209–217.
[38] F.B. Li, X.Z. Li, Photocatalytic properties of gold/gold ion-modified titanium dioxide for wastewater treatment, Appl. Catal. A: Gen. 228 (2002) 15–27.